Wetting layer of copper on the tantalum (001) surface

Maxime Dupraz, Roberta Poloni, Kitti Ratter, David Rodney, Maurizio de Santis, Bruno Gilles, Guillaume Beutier, Marc Verdier

Wetting layer of copper on the tantalum (001) surface

Maxime Dupraz,[1] Roberta Poloni,[1] Kitti Ratter,[1,2] David Rodney,[1,3]
Maurizio De Santis,[2] Bruno Gilles,[1] Guillaume Beutier,[1] and Marc Verdier[1]

[1] *Univ. Grenoble Alpes, CNRS, SIMAP, F-38000 Grenoble, France.*
[2] *Institut Néel, CNRS, F-38000 Grenoble, France.*
[3] *Institut Lumière Matière, Université Lyon 1, CNRS, UMR 5306, F-69622 Villerbanne, France.*

The hetero-epitaxial interface formed by copper deposited onto the tantalum (001) surface is studied by surface X-ray diffraction and *ab initio* calculations. The analysis of the crystal truncation rods reveals the presence of a wetting layer of copper made of two atomic planes pseudomorphic to the tantalum substrate, with the upper most atomic planes significantly deformed. These findings are in total agreement with the results of density functional theory calculations. The presence of the wetting layer confirms a Stranski-Krastanov growth mode and is thought to explain the extremely fast atomic diffusion of copper during the dewetting process in the solid state at high temperature.

PACS numbers: 68.35.bd,68.35.Md,61.05.C-

INTRODUCTION

Copper is nowadays a widely used interconnected metal in integrated circuits devices. However, the rapid diffusion of copper through silicon and its poor adhesion to silicon oxide led to the investigation of reliable diffusion barriers to isolate the copper interconnects from the silicon chips. Among the diffusion barrier metals, tantalum is one of the most interesting candidates and the past two decades have seen an increasing interest for the study of the Cu–Ta system[1–4]. On top of its technological interest, the Cu–Ta system is also a prime example of a strongly heterogeneous film-substrate system with almost zero mutual solubility[5], different crystal structure [face-centered cubic (fcc) Cu vs. body-centered cubic (bcc) Ta], and very different lattice parameters. An atomic scale understanding of the growth mode, structure and thermodynamic stability of Cu thin films on Ta substrates is thus of both fundamental and technological interest.

The Cu/Ta interface is a good example of a bi-metallic system with a Stranski-Krastanov (SK) growth mode[6] and can be described as a growth of three-dimensional (3D) islands on top of a thin wetting layer. The structure and morphology of the Cu/Ta interface is however difficult to predict and the study of the stability and wetting behavior of thin Cu films deposited on a Ta substrate has been the subject of several experimental investigations and controversial observations over the past few years. All studies agree that Cu thin films are metastable on Ta and tend to dewet into 3D structures, leaving a thin wetting layer: this general behavior has been observed on polycrystalline bcc Ta[7] and on single-crystal surfaces of the bcc[8] and β structures[9].

Most studies deal with the (110) surface of bcc tantalum, which is the dense plane of the stable structure. It has been established that ultrathin Cu films form a stable pseudomorphic (PM) layer when deposited on top of a Ta (110) substrate for a coverage up to 1.22 monolayers (ML)[10]. Additional Cu layers are unstable and dewet in the solid state at temperatures and with kinetics depending strongly on contamination[7,9] and on the film thickness[8]. On a clean Ta surface in a Ultra High Vacuum (UHV) environment a Cu monolayer is stable up to 1000 K, temperature at which diffusion into the polycrystalline bulk occurs[7]. It was shown experimentally[9] and with *ab initio* calculations[11] that when Cu films dewet from Ta(110) substrates, they leave a single stable monolayer on top of which 3D Cu islands form. The crystallographic orientation of the dewetted copper on Ta(110) follows the Nishiyama-Wassermann relationship: Ta(110)[110]//Cu(111)[112][8].

The growth mode and wetting behavior of Cu thin films on Ta(001) are not well documented. The main experimental UHV investigation, performed by Venugopal *et al.*, reported the dewetting of Cu thin films deposited on Ta(001)[8]. They observed, by X-ray diffraction, both the (111) and (001) out-of-plane orientations of the Cu islands and found, based on the morphologies observed by Scanning Electron Microscopy (SEM), that the latter is largely predominant. On the other hand, Francis *et al.* observed a strong (111) texture for copper thin films sputtered on Ta(001)[12]. We also reported the dewetting of highly strained Cu islands with Cu(001)[110]//Ta(001)[100] orientation relationship[13]. Venugopal *et al.* evidenced a remaining wetting layer between the dewetted islands, with a thickness estimated to less than 5 Å, corresponding to 1 or 2 ML[8].

There is, to our knowledge, no experimental determination of its structure to date, but several numerical works have addressed the question. A first study employing molecular dynamics (MD) predicted that the Cu(111)/Ta(001) interface is more stable than Cu(001)/Ta(001) and Cu(110)/Ta(001) interfaces[14]. More relevant to the dewetting of a single Cu thin film, Lazic *et al.* performed MD calculations of the deposition of Cu on a Ta(001) surface, and found a fcc structure with (111) texture from the third Cu ML, on top of a PM ML and a complex intermediate ML[15]. Only Hashibon *et al.*[16] developed cross potentials for Cu–Ta from *ab initio* calculations, to describe the dewettting of Cu

on the Ta(110) surface. There is thus so far no numerical work predicting the Cu(001)[110]//Ta(001)[100] orientation relationship evidenced by Venugopal *et al.* and Beutier *et al.*[8,13]. We note that in the works mentioned above, *ab initio* calculations using the density functional theory (DFT) were not directly employed to assess the stability of various interfaces, but used indirectly to build interatomic potentials for MD simulations.

In this study, we used Surface X-Ray Diffraction (SXRD) and DFT calculations to address the presence and structure of a wetting layer of Cu on the Ta(001) surface. We measured SXRD *in situ* while depositing and dewetting a thin Cu layer on a Ta(001) surface. The measurements show unambiguously the presence of two PM Cu layers. The interplanar spacing between the Cu layers and the uppermost Ta layers is also determined. DFT calculations in the local density approximation were used to calculate the excess interface energy of a variety of configurations with different numbers of Cu ML and different structures. A very good agreement is found between both approaches.

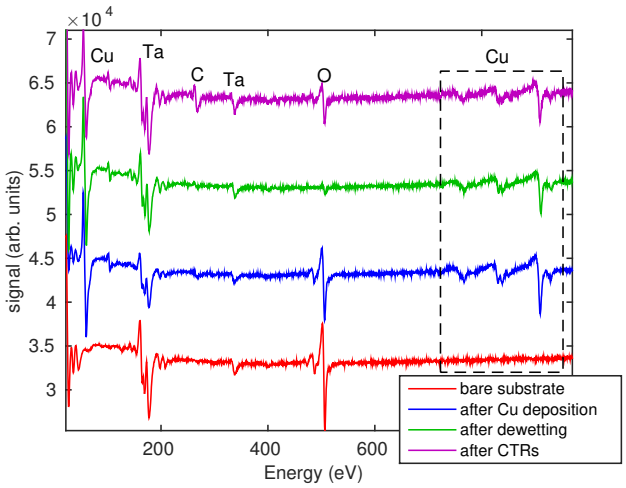

FIG. 1. Auger spectra at various stages of the experiment (here: data set D).

I. SURFACE X-RAY DIFFRACTION

SXRD is a powerful probe of the structure of crystalline surfaces[17]. Sharp interfaces give rise to Crystal Truncation Rods (CTR) in reciprocal space[18] that are particularly useful to evidence PM wetting layers[19]. Indeed, the scattering amplitude from PM layers is enhanced by interference with the scattering amplitude from the substrate in the vicinity of the in-plane Bragg reflections of the latter, allowing a quantitative determination of the number of atomic layers and their interplanar spacing.

The experiment was carried out at beamline BM32 of the European Synchrotron Radiation Facility (ESRF), on the SUV end station[20]. The latter consists of an UHV chamber fully equipped for sample preparation, mounted on a Z-axis diffractometer[21]. Further degrees of freedom are available to align the sample. While the deposition of copper by molecular beam epitaxy (MBE) and the dewetting could be performed *in situ*, the preparation of the Ta(001) surface requires flash annealing at temperatures above 2000 K, which cannot be done with the set-up of the beamline. The surface preparation was thus performed in the UHV chamber of the SIMaP laboratory and then transferred to the beamline chamber.

A high purity (more than 99.9999%) Ta crystal, cut and polished to less than 0.1° along the (001) plane, was purchased from MaTecK GmbH. The surface was prepared by repeated cycles of Argon sputtering and flash annealing above 2000 K to remove oxygen and carbon contamination[22]. The atomic flatness of the surface was monitored by Low-Energy Electron Diffraction (LEED), and the minimum level of oxygen or carbon contamination was checked by X-ray Photoelectron Spectrometry (XPS). A protective 5 nm copper layer was then deposited to cover the Ta surface during the transfer from the laboratory chamber to the UHV beamline chamber, where it was removed by evaporation above 1300K. The transfer was done mostly in primary vacuum, with a short exposure (a few seconds) to air. We were thus able to obtain a clean Ta bare substrate surface (FIG. 1).

Four data sets (thereafter called A, B, C, and D) were collected during two experimental sessions. The conditions of preparation of the Ta surface, and the Cu deposition and dewetting differed for the four data sets. The relevant parameters are summarized in Table I. The same substrate was used for the (A,B,C) data set according to the procedure detailed above. For data set D, the substrate from experiment C was reused and thus did not undergo a high temperature flash annealing preparation. The remaining copper was evaporated *in situ* until a clean surface was obtained (3 minutes at 1370 K). A characteristic signature of Oxygen can be seen in the Auger spectrum of the bare Ta substrate, at 510 eV. It corresponds to about a third of an atomic layer. These are adsorbed Oxygen atoms, responsible for a surface reconstruction[23], that desorb during the dewetting (green line in FIG. 1).

Starting from the bare substrate at room temperature, a few (exact numbers depending on data sets) ML of copper were deposited *in situ* at low rate (∼5 min/ML). For the data set A only, the Cu thin film was then sputtered by argon for 20 minutes. The dewetting was then performed *in situ* at high temperature (1020 – 1070 K), using the furnace of the sample stage. The temperature was monitored with a pyrometer and the base pressure into the chamber was carefully checked to avoid copper evaporation from the surface. The dewetting was monitored by the rocking curve of the Cu 111 reflections: the beginning of dewetting into islands yield a sharp increase of the peak intensity and a decrease of the rocking curve width. After dewetting, the Auger spectra show

Data set	Session	substrate restauration	Cu thickness	Argon sputtering	Dewetting and maturation
A	April 2014	yes	∼9 nm	yes	20 min. at 1020K
B	Sept 2014	yes	22 ML (∼4 nm)	no	5 min. at 1070K + 1 min. at 1100K
C	Sept 2014	yes	22 ML (∼4 nm)	no	5 min. at 1070K + 1 min. at 1100K
D	Sept 2014	no	3 ML	no	1 min. at 1050K

TABLE I. Sample preparation parameters for the four data sets.

	Oxygen contamination		Carbon contamination					
Data set	before CTR	after CTR	before CTR	after CTR	Age at start of $11L$ CTR	$\Delta(11L)$	Age at start of $10L$ CTR	$\Delta(10L)$
A	very low	medium	no	strong	3.5 h	0.073	0.5 h	0.116
B	low	medium	no	low	2 h	0.103	3.5 h	0.099
C	low	medium	no	low	0.5 h	0.089	3.5 h	0.079
D	low	medium	no	medium	0.5 h	0.078	3.5 h	0.083

TABLE II. Contamination of the surface before and after the CTR measurements. The age of the sample is counted from the end of the dewetting.

an increase of the ratio between low energy electron and high energy electrons (FIG. 1). This can be explained by the presence of a thin wetting layer between the islands. The Cu(920 eV)/Cu(60 eV) intensity ratio does not increase despite the dewetting at high temperature, which suggests that diffusion of copper into the substrate can be excluded[7]. At this stage, the Oxygen signature has disappeared, due to the desorption of the adatoms upon heating[23]. No other contamination is evidenced yet.

The Auger spectra were remeasured after the CTRs measurements, evidencing oxygen and carbon contaminations of more or less importance depending on the data set (FIG. 1). The level of contamination is summarized in Table II. Because of the slow contamination, the delay between the dewetting and the CTR measurements could be an important parameter. This issue can be addressed by comparing the four data sets.

The X-ray source is a bending magnet and the monochromator is a Si(111) double crystal, with the second crystal bent to give sagittal focusing on the sample. The vertical focusing is provided by a mirror, resulting in a spot size of about 0.4×0.3 mm^2. The measurements were performed at photon energy of 22 keV. The detector was a Maxipix camera[24]. In order to reduce the Thermal Diffuse Scattering from the bulk, the penetration of X-rays into the sample has to be kept as small as possible. This can be achieved by using a low glancing angle α of the incoming X-ray beam. In this experiment alpha was set to 0.6°, a value about three times the critical angle of total external reflection (0.194° for Ta at 22 keV).

The atomic structure of the surface can be determined from the structure factors measured along the CTRs, extracted from the integrated intensities measured by scanning across the CTRs with the angle ω[20,25] over a range of ±5°. This relatively large range ensures an accurate measurement of the background level. The CTRs are thereafter indexed in the reciprocal lattice units (r.l.u.) of bcc tantalum, with a (001) surface. The $10L$ and $11L$ CTRs ($0<L<3$) were measured for each data set. All measurements were averaged over two equivalent CTRs, based on the overall tetragonal symmetry of the surface. The agreement factor Δ (average-normalized variance) between equivalent CTRs is reported in Tab. II. The error bars shown in the figures below are calculated as a mix of the variance between equivalent reflections and of the statistical error[26].

For all data sets, clear interferences can be seen on the CTRs, revealing the presence of epitaxial layers (FIG. 2). A straitforward conclusion is the absence of amorphisation of copper, such as observed by Kwon *et al* at the interface with β-tantalum upon annealing[27]. Consistently with our result, they do not see such amorphisation but an atomically sharp interface with bcc tantalum, of which the crystallographic orientation is not given.

Auger spectroscopy revealed a strong carbon contamination in the data set A after the CTR measurements. This is clearly seen on both CTRs from this data set, which show less contrasted features than the other three data sets and a shift of the minimum of the $11L$ CTR (FIG. 2). The impact of carbon contamination seems to be lower on the $10L$ CTR, which was measured shortly after dewetting, while the $11L$ was measured three hours later. Such contamination could decrease the coherent fraction of the wetting layer. The other three data sets show very similar CTRs. The effect of oxygen contamination is difficult to evaluate, because the contamination level is similar for the four data sets.

After the last SXRD measurement, the surface of the sample has been imaged by optical and atomic force microscopy and confirm the dewetting of the excess copper into 3D islands similar to those observed in[8,13]. Their density is very low, in agreement with the small quantity of copper deposited for this data set (estimated to 3 ML, among which only one dewetted), with an average 30 μm distance between islands.

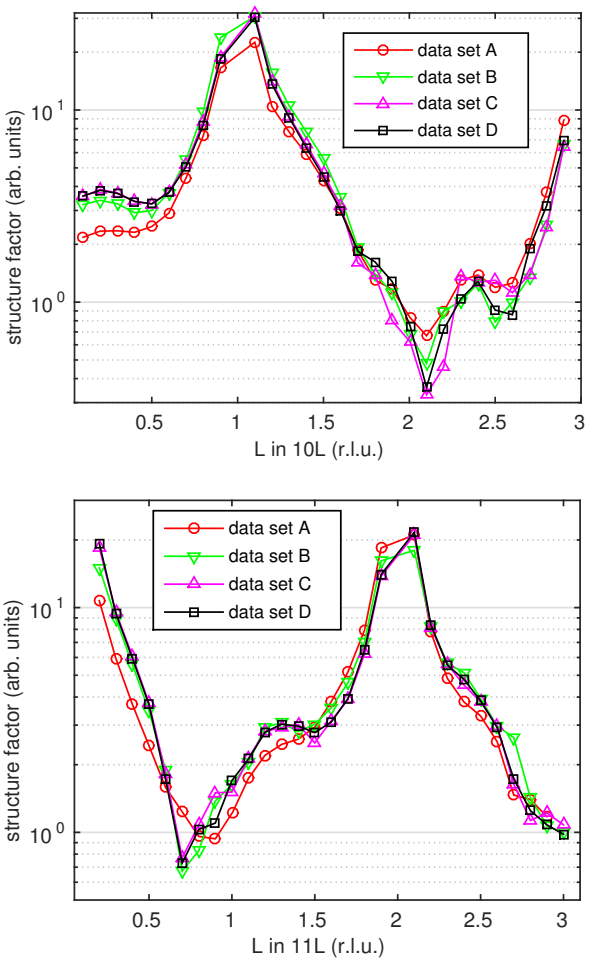

FIG. 2. $10L$ and $11L$ CTRs for four different data sets with different states of surface contamination. Error bars have been omitted to facilitate the visualization.

II. DENSITY FUNCTIONAL THEORY CALCULATIONS

From the measured CTRs, the precise determination of the structure of the interface is in principle obtained by the fitting of the experimental data. DFT calculations were performed to gain further insight in the experimental results. The agreement between the interfaces predicted from the experimental data and the DFT calculations is quantified and discussed in details.

Total energy calculations were performed using the local-density approximation to the exchange and correlation and norm conserving Martins-Troullier pseudo potentials[28] as implemented in the PWSCF code[29]. The wave function and charge density cutoffs were taken as 90 Ry and 360 Ry, respectively. Atomic relaxation was performed until atomic forces were less than 0.03 eV/Å. The bulk structures of bcc Ta and fcc Cu were fully optimized using a 12x12x12 Monkhorst-Pack grid[30] for the integration of the irreducible Brillouin zone leading to a_{Cu} = 3.554 Å and a_{Ta} = 3.235 Å. These values are about 2% smaller than the experimental values (3.615 Å and 3.301 Å respectively at room temperature), consistent with the local density approximation. Importantly, the ratio of calculated lattice parameters is $(a_{Cu} - a_{Ta})/a_{Ta} = 9.9\%$, in good agreement with the experimental value (9.5%). The slab calculations of a few PM Cu layers described in the following section employed a 12x12x1 Monkhorst-Pack grid.

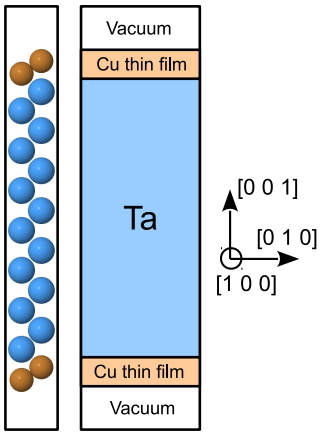

FIG. 3. Slab configuration to model the relaxation of a varying number of PM Cu layers.

In order to determine the stability and structure of a Cu thin film on Ta(001), interfaces containing 1 to 6 PM layers were modeled using a periodic slab configuration (FIG. 3). It consists of a stack of 14 Ta (001) planes covered by 1 to 6 bcc Cu layers on both sides, leading to two equivalent Cu/Ta interfaces. Each layer was modeled using only one atom per unit cell by taking advantage of the in-plane periodic boundary conditions. A thick vacuum region of about 15 Å was added along z between the two Cu films in order to ensure a negligible interaction between the two free surfaces. The structural relaxation was computed by relaxing the z coordinate of all atoms of the supercell.

The thermodynamical stability of Cu thin films was evaluated by computing the excess interface energy as the energy difference between the fully relaxed configuration for each model and the configuration with the same number of atoms in their bulk environments. It can thus be written as:

$$\gamma = \frac{E_{supercell} - (E^{Ta}_{bulk} + E^{Cu}_{bulk})}{2A} \quad (1)$$

where $E_{supercell}$ is the total energy of the slab calculation and A is the surface area (considered twice for the two Cu/Ta interfaces). The excess interface energy described in Eq. 1 is the sum of the film/substrate interface energy, γ_i, and the free surface energy of the thin film, γ_f, *i.e.* $\gamma = \gamma_i + \gamma_f$. The elastic strain energy contribution (estimated to $1/2M\epsilon^2 h$, with M the biaxial in plane elastic modulus, ϵ the strain and h the thickness) which is im-

N	0	1	2	3	4	5	6
γ (J/m^2)	3.18	2.50	2.19	2.63	2.78	3.13	3.32

TABLE III. Calculated excess interface energy γ as a function of the number N of PM Cu layers on the Ta(001) surface.

plicitly contained in Eq. 1 increases with the number of layers of the film and quickly dominates the trend.

In order to evaluate the stability and growth mode of a film on a substrate, the energy difference δ between the free surface and the interface configurations needs to be considered. This is given by[31,32]:

$$\delta = \gamma_i + \gamma_f - \gamma_s = \gamma - \gamma_s \qquad (2)$$

where γ_s is the free surface energy of the substrate. For $\delta < 0$ the film/substrate interface is thermodynamically stable and a complete coverage of the substrate by the thin film is expected. When this condition is satisfied, a layer-by-layer growth, known as the Frank-van-der-Merwe mode is observed[33,34]. Starting from $\delta = 0$, the Stranski-Krastanov growth is obtained, which corresponds to a 3D growth on top of the thin film. The excess interface energies calculated up to 6 Cu PM layers are reported in Tab. III.

The computed free surface energy, γ_f, of Ta(001) is 3.18 J/m^2 which is larger than the experimental value of 2.5 J/m^2[35], but close to other theoretical values of 3.10 J/m^2[36] and 3.14 J/m^2[37]. This results in $\delta < 0$ for up to 5 PM layers. As mentioned above, the increase in γ found for increasing number of layers, reflects the increase in strain energy.

The configuration with 2 PM layers on top of the substrate has the lowest energy and is therefore the most stable configuration for a thin film of Cu on Ta(001) while 1, 3, 4 and 5 Cu PM layers are metastable. The calculations indicate that a Frank-van-der-Merwe growth mode is expected up to 5 PM layers above which a Stranski-Krastanov mode is expected. This result is consistent with experimental data which reported the presence of 1 or 2 wetting layers[8]. For all the PM configurations, the high in-plane tensile strain induces a compensative high out-of-plane compressive strain among the Cu layers. The configuration with 2 PM layers is studied in more details in the next section.

As a comparison, we computed the wetting behavior of Cu on Ta(110) and found that 1 PM layer is the most stable configuration thermodynamically, while 2 PM layers are metastable. The computed free surface energy of Ta(110) is 2.98 J/m^2 while the excess interface energy is 2.34 J/m^2 and 2.74 J/m^2, respectively. This result contradicts the findings of Ref.[11], where none of the PM configurations were predicted to be stable on the Ta(110) surface, but is consistent with experimental observations[7,10].

We also considered the case of Cu fcc layers on top of the Ta substrate or on top of the PM Cu layers. These configurations, requiring a significantly larger cell and larger computing time, did not converge to acceptable structures. For instance, the configuration with a single Cu fcc layer on top of the Ta substrate tends to form a PM layer. Other cases involving PM Cu layers result in an out-of-plane modulation due to the periodic boundary conditions. It is therefore impossible to extract the excess interface energy of these configurations. We note that bcc copper is not uncommon at interfaces[38,39].

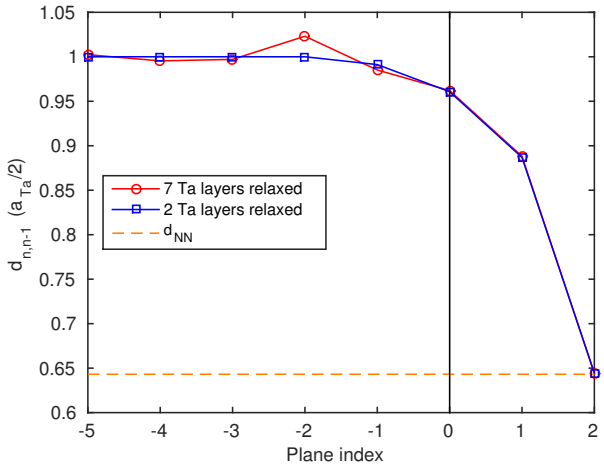

FIG. 4. Interplanar spacing versus plane index for 2 and 7 relaxed Ta planes, normalized to the value in bulk tantalum ($a_{Ta}/2$). The numerical values for 7 relaxed planes are given in Table IV. The last tantalum plane is at index 0; indexes 1 and 2 correspond to copper planes. d_{NN} is the value of $d_{1,2}$ that conserves the nearest-neighbor distance of the bulk copper.

The interplanar distances in the DFT configuration with two PM layers are shown in FIG. 4. The high in-plane misfit strain results in reduced interplanar distances along the (001) direction by 11% for the Ta–Cu interface and by 36% for the Cu–Cu bilayer, with respect to the interlayer spacing in bulk Ta ($a_{Ta}/2$). Such a huge tetragonal distortion has been observed in thick films in the case of the Bain transformation[40]. Here it is not a relevant parameter of stability since we deal with only two atomic layers, each of them being at an interface. It is more relevant to consider the Cu–Cu nearest-neighbor distance in the Cu bilayer. With an interplanar distance of $d_{1,2} = 1.042$ Å, the latter is:

$$d_{Cu-Cu} = \sqrt{2\left(\frac{a_{Ta}}{2}\right)^2 + d_{1,2}^2} \approx 2.513 \text{ Å} \qquad (3)$$

By comparison, the nearest-neighbor distance in fcc copper ($a_{Cu}/\sqrt{2}$) is also 2.513 Å. (The real experimental value is 2.556 Å at room temperature.) We see that, in absence of a third layer, the body-centered tetragonal pseudomorphic stacking allows the copper atoms to keep an interatomic distance similar to that in the bulk fcc value, thus minimizing the elastic energy. A third PM layer would cause a large frustration either of the

first-neighbor distance or of the second-nearest-neighbor distance, hence the increase of energy above 2 PM layers.

The interplanar distance at the interface is of 1.436 Å, resulting in a Cu–Ta interatomic distance:

$$d_{Cu-Ta} = \sqrt{2\left(\frac{a_{Ta}}{2}\right)^2 + d_{0,1}^2} \approx 2.701 \text{ Å} \qquad (4)$$

The tantalum atoms are also affected by the presence of neighboring Cu atoms, and a strong relaxation of the first three tantalum interlayer distances at the interface is observed. The first two are compressed by 3.9% and 2.5% for $d_{-1,0}$ and $d_{-2,-1}$ respectively, while the third one is increased by 2.3%. The strain below the first three planes nearly vanishes: the spacing between Ta_{-4}, and Ta_{-5}, Ta_{-5} and Ta_{-6}, and Ta_{-6} and Ta_{-7} is indeed close to the bulk nominal value of Ta (respective variations of -0.3%, -0.45% and 0.24%).

III. COMPARISON BETWEEN DFT CALCULATIONS AND SXRD DATA

According to the DFT calculations, the thermodynamically most stable configuration is 2 PM copper layers on top of the Ta(001) surface. The agreement between DFT calculations and SXRD measurements was checked by computing the structure factors using the DFT configurations and comparing them with the experimental structure factors. These calculations were performed in the kinematical approximation of X-ray diffraction using the software ROD[41] according to:

$$F_{tot}(HKL) \propto |F_b(HKL) + F_s(HKL)| \qquad (5)$$

where HKL are the Miller indices. The bulk structure factor $F_b(HKL)$ is calculated for a perfect semi-infinite crystal of tantalum, and the surface structure factor $F_s(HKL)$ is calculated using all the atoms of the model, including the tantalum atoms belonging to the seven layers just below the copper layers:

$$F_s(HKL) = \sum_j f_j e^{2i\pi(Hx_j+Ky_j+Lz_j)} e^{-\frac{B_j(H^2+K^2+L^2)}{4a_{Ta}^2}} \qquad (6)$$

where f_j is the atomic scattering factor of atom j, $(xyz)_j$ its position in fractional coordinates and B_j its isotropic Debye-Waller parameter. The scale factor in Equation 5 includes a roughness factor calculated within the β model[42].

FIG. 5 presents several comparisons between CTRs measured from the cleanest Ta surfaces (data sets A and D), and the simulated CTRs for 1, 2 and 3 PM Cu layers. For both the $11L$ and $10L$ CTRs, the best agreement is found for 2 PM layers. We note that the structure factors are systematically overestimated at high L values. Despite this discrepancy, the 2 PM model reproduces well all the features of the experimental data, unlike the other models.

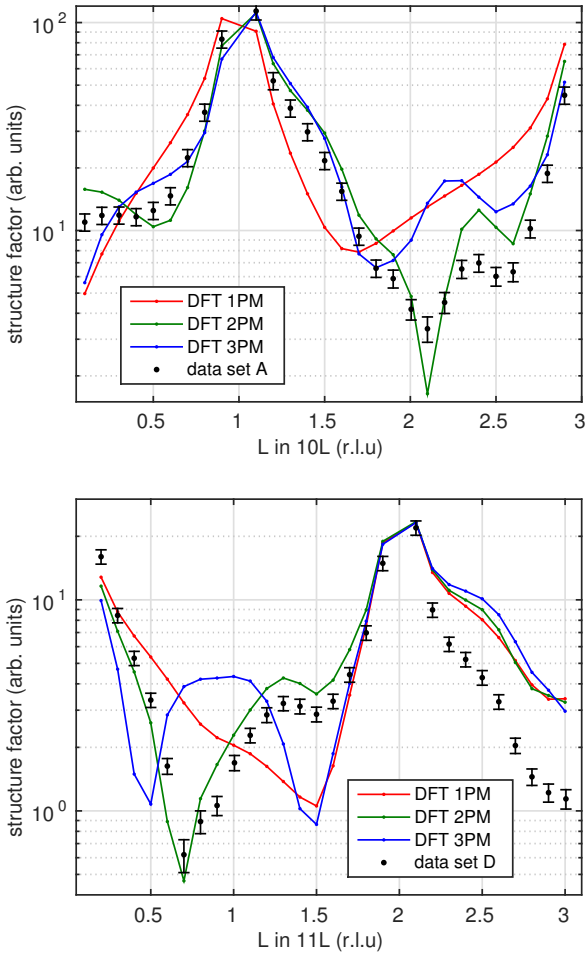

FIG. 5. $10L$ (a) and $11L$ (b) structure factors obtained using DFT configurations with a varying number of PM Cu layers, compared with experimental data.

To clarify the importance of the Ta relaxation, the structure factors of four different systems were calculated and compared to the experimental data. In the first case, the relaxation of the Cu atoms was taken into account whereas the atomic positions for Ta were equal to their nominal bulk values. In the second, third and fourth cases, the relaxation of Cu was taken in account and the relaxation of the Ta atoms was restricted respectively to 2, 3 and 7 Ta planes. As shown in FIG. 6, for up to 3 Ta planes, the number of Ta planes taken into account for relaxation has a very strong influence on the calculated structure factors. In all cases and independently of the number of relaxed Ta planes, the positions of the minima of amplitude are reproduced accurately for both CTR. However, the agreement between the calculated structure factors and the experimental data is rather poor for less than 3 relaxed Ta plane. For the 10L CTR, the four configurations reproduce the dip of intensity around L = 2.1 r.l.u., however the bump which is observed in the $2.2 < L < 2.6$ r.l.u. region is reproduced accurately only

when at least 3 Ta planes are relaxed. Similar conclusions can be drawn for the $11L$ CTR where the configurations with 0 and 2 relaxed Ta planes fail to reproduce the curve inflection in the $1 < L < 1.5$ r.l.u. and $2.3 < L < 2.7$ r.l.u. regions. The dip of amplitude for $L = 0.7$ r.l.u. is also strongly overestimated when the number of relaxed Ta planes is less than three. These remarks allow to set an upper limit for the resolution obtained on the lattice relaxation: the relaxation of the third Ta layer, of 0.03 Å, is clearly seen. The simulated CTR for 3 and 7 relaxed Ta planes exhibit a remarkable similarity. This suggests that most of the relaxation occurs within the upper three Ta planes and is consistent with the small value of displacements found for the Ta planes further away from the interface. The good agreement with the experimental data obtained by relaxing the atomic layers is a strong evidence supporting the absence of non-pseudomorphic layers (fcc) on top of the pseudomorphic layers, because additional layers, even though invisible on the CTRs originating from the Ta reciprocal lattice points, would modify the interplanar spacing.

Finally, the DFT structure of the fully relaxed interface with 2 PM layers was employed as the starting model to fit the experimental data, by relaxing the following parameters: the interplanar spacings, the Debye-Waller factors, and the β value of the roughness factor[42]. ROD also allows to release the surface fraction of the coherent layer. Attempts to do so lead to values very close to 1 (full coverage) without significant improvements of the fits, and the results presented here were performed without releasing this parameter. Indeed, the total amount of deposited copper exceeded 2 PM and there is no reason to think that the surface coverage is not full. The 8 experimental data sets (2 CTRs for each of the 4 samples) were fitted independently. FIG. 7 shows a comparison between two experimental curves and the calculations before and after fitting. The interlayer spacings resulting from the fits are given in Tab. IV, averaged by CTR over the 4 samples, and shown in FIG. 8. Alternative starting guesses were tried, such as using $a_{Ta}/2$ for the Ta–Ta interlayer distances, and the fits converged to the same values well within the error bars. Remarkably, the final fit parameters are very close to the DFT predictions. In particular, the SXRD data confirm the relaxation of the three upper atomic layers of tantalum. For each CTR, the dispersion of the values of the interlayer spacings is very small, suggesting the small influence of the surface contamination. There is actually more dispersion between the values provided by the two CTRs. This systematic error is also observed on the roughness parameter β, which is found of the order of 1% for the $10L$ CTR and of the order of 10% for the $11L$ CTR. In addition to the interlayer spacings, the isotropic Debye-Waller factors of the 4 upper layers (the 2 Cu layers and 2 Ta layers) are relaxed for the fits. The fits yield isotropic displacement parameters of 3.8, 4.7, 5.3, 11.1 Å^2 from bottom to top, with dispersions close to 100%. These large values are needed to reproduce the fall of the experimental data at large L. We infer that they point to a large static disorder. The surface contamination and its increase with time have probably a major role in determining such high values.

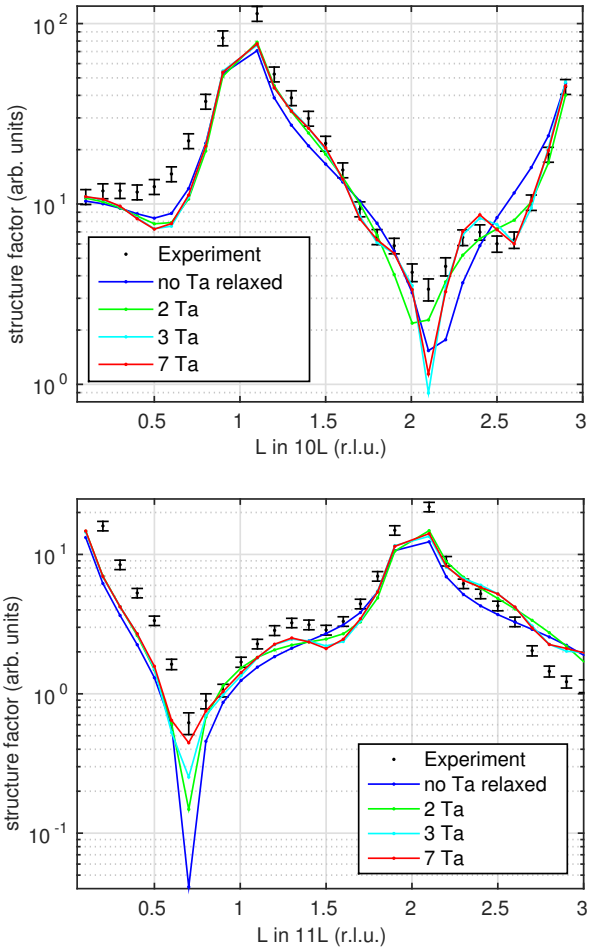

FIG. 6. Influence of the number of relaxed Ta planes in the DFT calculations on the calculated $10L$ and $11L$ structure factors.

CONCLUSIONS

This study of the Cu/Ta(001) interface, combining SXRD measurements and DFT calculations in excellent mutual agreement, demonstrates the presence of two pseudomorphic layers of copper wetting on the Ta(001) surface after dewetting of excess copper. This result is robust for a small contamination of the surface by carbon and oxygen. The measurements performed with the lowest contamination were used to fit the surface structure and to determine the interplanar distances. The two copper PM layers are in body-centered tetragonal stacking and have interplanar spacing of $d_{1,2} = 1.05$ Å$\pm$ 0.05 Å, which allows to maintain the same nearest-neighbor distance as in the bulk (fcc). This configuration, which min-

Interlayer spacing $[/(a_{Ta}/2)]$	DFT value	$10L$	$11L$	SXRD average
$d_{-6,-5}$ (Ta–Ta)	1.000	1.000*	1.000*	1.000*
$d_{-5,-4}$ (Ta–Ta)	0.995	0.995*	0.995*	0.995*
$d_{-4,-3}$ (Ta–Ta)	0.997	0.997*	0.997*	0.997*
$d_{-3,-2}$ (Ta–Ta)	1.023	1.020±0.001	1.020±0.001	1.020±0.001
$d_{-2,-1}$ (Ta–Ta)	0.985	0.985±0.002	0.983±0.001	0.984±0.003
$d_{-1,0}$ (Ta–Ta)	0.962	0.964±0.002	0.963±0.009	0.964±0.009
$d_{0,1}$ (Cu–Ta)	0.888	0.903±0.006	0.85±0.03	0.88±0.05
$d_{1,2}$ (Cu–Cu)	0.644	0.62±0.03	0.65±0.01	0.64±0.03

TABLE IV. Interlayer spacings: DFT values and refined fit parameters. Error bars for the CTR fits corresponds to the largest deviation to the mean in the 4 data sets (or in the 4×2 data sets for the average value). * value not relaxed for the fits.

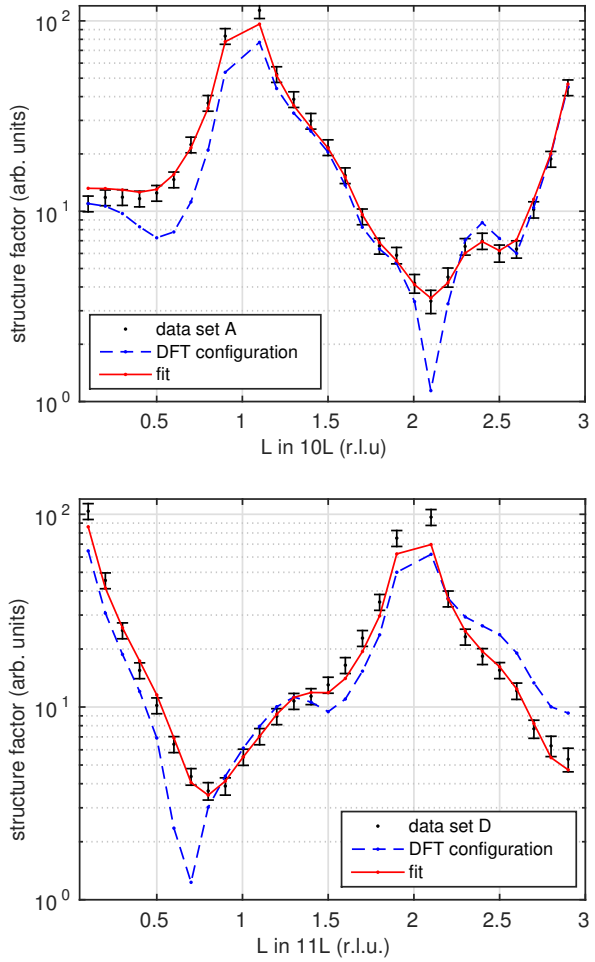

FIG. 7. $10L$ and $11L$ CTRs structure factors, before and after fitting.

imizes the elastic energy in the Cu – Cu bonds, is possible only in the absence of a third layer of copper. This feature is possibly one reason that explain the anomalously fast diffusion of Cu atoms during solid-state dewetting on Ta(001). Indeed, the dewetting occurs not directly on the Ta(001) surface, but on top of two PM layers.

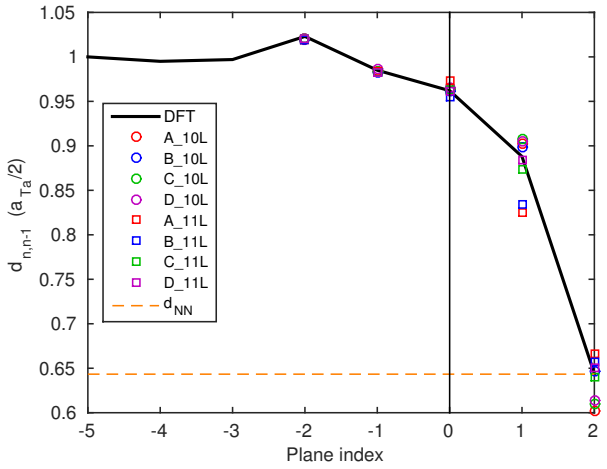

FIG. 8. Interlayer spacing resulting from the 8 experimental curves. d_{NN} is the value of $d_{1,2}$ that conserves the nearest-neighbor distance of the bulk copper. The values are given in unit of the interlayer spacing in the bulk tantalum.

ACKNOWLEDGMENTS

Beamtime is acknowledged at the French CRG BM32 beamline of the ESRF. Calculations were performed using computer resources from GENCI under the CINES grant C2016097211. This work was supported by the French ANR project MECANIX (ANR-11-BS10-0014).

[1] K. Holloway, P. M. Fryer, C. Cabral Jr, J. Harper, P. Bailey, and K. Kelleher, Journal of Applied Physics **71**, 5433 (1992).

[2] T. Laurila, K. Zeng, J. K. Kivilahti, J. Molarius, and I. Suni, Journal of Applied Physics **88**, 3377 (2000).

[3] H. Kim, T. Koseki, T. Ohba, T. Ohta, Y. Kojima, H. Sato, and Y. Shimogaki, Journal of The Electrochemical Society **152**, G594 (2005).

[4] C. M. Müller and R. Spolenak, Thin Solid Films **598**, 276 (2016).

[5] M. Singleton, J. Murray, and P. Nash, "Binary alloy phase diagrams," (American Society for Metals, Metals Park, OH, 1986) p. 181.

[6] J. A. Rodriguez and D. W. Goodman, The Journal of Physical Chemistry **95**, 4196 (1991).

[7] L. Chen, N. Magtoto, B. Ekstrom, and J. Kelber, Thin Solid Films **376**, 115 (2000).

[8] V. Venugopal and B. Thijsse, Thin Solid Films **517**, 5482 (2009).

[9] F. Fillot, Z. Tőkei, and G. Beyer, Surface Science **601**, 986 (2007).

[10] W. K. Kuhn, R. A. Campbell, and D. W. Goodman, The Journal of Physical Chemistry **97**, 446 (1993).

[11] A. Hashibon, C. Elsässer, Y. Mishin, and P. Gumbsch, Physical Review B **76**, 245434 (2007).

[12] M. F. Francis, M. N. Neurock, X. W. Zhou, J. J. Quan, H. N. G. Wadley, and E. B. Webb, Journal of Applied Physics **104**, 034310 (2008), http://dx.doi.org/10.1063/1.2968240.

[13] G. Beutier, M. Verdier, G. Parry, B. Gilles, S. Labat, M.-I. Richard, T. Cornelius, P.-F. Lory, S. V. Hoang, F. Livet, *et al.*, Thin Solid Films **530**, 120 (2013).

[14] H. R. Gong and B. X. Liu, Applied Physics Letters **83** (2003).

[15] I. Lazić, P. Klaver, and B. Thijsse, Physical Review B **81**, 045410 (2010).

[16] A. Hashibon, A. Y. Lozovoi, Y. Mishin, C. Elsässer, and P. Gumbsch, Physical Review B **77**, 094131 (2008).

[17] I. K. Robinson and D. J. Tweet, Reports on Progress in Physics **55**, 599 (1992).

[18] S. R. Andrews and R. A. Cowley, Journal of Physics C: Solid State Physics **18**, 6427 (1985).

[19] M. Ball, C. Lucas, N. Markovic, V. Stamenkovic, and P. Ross, Surface Science **518**, 201 (2002).

[20] R. Baudoing-Savois, M. D. Santis, M. Saint-Lager, P. Dolle, O. Geaymond, P. Taunier, P. Jeantet, J. Roux, G. Renaud, A. Barbier, O. Robach, O. Ulrich, A. Mougin, and G. Bérard, Nuclear Instruments and Methods in Physics Research Section B: Beam Interactions with Materials and Atoms **149**, 213 (1999).

[21] J. M. Bloch, Journal of Applied Crystallography **18**, 33 (1985).

[22] R. Musket, W. McLean, C. A. Colmenares, D. Makowiecki, and W. Siekhaus, Applications of Surface Science **10**, 143 (1982).

[23] H. Yamazaki, K. Sakamoto, A. Fujii, and T. Kamisawa, Surface Science **563**, 41 (2004).

[24] C. Ponchut, J. Rigal, J. Clément, E. Papillon, A. Homs, and S. Petitdemange, Journal of Instrumentation **6**, C01069 (2011).

[25] E. Vlieg, Journal of Applied Crystallography **30**, 532 (1997).

[26] E. Vlieg, *From beam time to structure factors, including a concise guide to ANA and AVE* (2012).

[27] K.-W. Kwon, H.-J. Lee, and R. Sinclair, Applied Physics Letters **75** (1999).

[28] N. Troullier and J. L. Martins, Physical review B **43**, 1993 (1991).

[29] P. Giannozzi, S. Baroni, N. Bonini, M. Calandra, R. Car, C. Cavazzoni, D. Ceresoli, G. L. Chiarotti, M. Cococcioni, I. Dabo, *et al.*, Journal of Physics: Condensed Matter **21**, 395502 (2009).

[30] H. J. Monkhorst and J. D. Pack, Physical Review B **13**, 5188 (1976).

[31] L. B. Freund and S. Suresh, *Thin film materials: stress, defect formation and surface evolution* (Cambridge University Press, 2004).

[32] M. Wuttig and X. Liu, "Epitaxy-stabilized structures," in *Ultrathin Metal Films: Magnetic and Structural Properties* (Springer Berlin Heidelberg, Berlin, Heidelberg, 2004) pp. 125–207.

[33] F. C. Frank and J. H. van der Merwe, Proceedings of the Royal Society of London. Series A, Mathematical and Physical Sciences (1949).

[34] J. H. Van Der Merwe, Journal of Applied Physics **34**, 123 (1963).

[35] W. Tyson and W. Miller, Surface Science **62**, 267 (1977).

[36] L. Vitos, A. Ruban, H. L. Skriver, and J. Kollar, Surface Science **411**, 186 (1998).

[37] F. Aqra and A. Ayyad, Applied Surface Science **257**, 6372 (2011).

[38] C. Schmidt, F. Ernst, M. W. Finnis, and V. Vitek, Phys. Rev. Lett. **75**, 2160 (1995).

[39] H. Kung, Y.-C. Lu, A. J. Griffin, M. Nastasi, T. E. Mitchell, and J. D. Embury, Applied Physics Letters **71**, 2103 (1997).

[40] J. Buschbeck, I. Opahle, M. Richter, U. K. Rößler, P. Klaer, M. Kallmayer, H. J. Elmers, G. Jakob, L. Schultz, and S. Fähler, Phys. Rev. Lett. **103**, 216101 (2009).

[41] E. Vlieg, Journal of Applied Crystallography **33**, 401 (2000).

[42] I. K. Robinson, Physical Review B **33**, 3830 (1986).